Physics of Plasmas ARTICLE scitation.org/journal/php

Superthin current sheets supported by anisotropic electrons

Cite as: Phys. Plasmas **27**, 082904 (2020); doi: 10.1063/5.0018063
Submitted: 11 June 2020 · Accepted: 3 August 2020 ·
Published Online: 18 August 2020

S. R. Kamaletdinov,[1,2,a)] E. V. Yushkov,[1,2,b)] A. V. Artemyev,[2,3,c)] A. S. Lukin,[2,4,d)] and I. Y. Vasko[2,5,e)]

AFFILIATIONS

[1]Department of Physics, Moscow State University, 1-2 Leninskie Gory, Moscow 119991, Russia
[2]Space Research Institute of the Russian Academy of Sciences (IKI), 84/32 Profsoyuznaya Str., Moscow 117997, Russia
[3]Department of Earth, Planetary, and Space Sciences, University of California, 595 Charles E Young Dr E, Los Angeles, California 90095, USA
[4]Faculty of Physics, National Research University Higher School of Economics, 21/4 Staraya Basmannaya Ulitsa, Moscow 105066, Russia
[5]Space Sciences Laboratory, University of California at Berkeley, 7 Gauss Way, Berkeley, California 94720, USA

[a)]Author to whom correspondence should be addressed: serjesmail@yandex.ru
[b)]Electronic mail: yushkov.msu@mail.ru
[c)]Electronic mail: aartemyev@igpp.ucla.edu
[d)]Electronic mail: as.lukin.phys@gmail.com
[e)]Electronic mail: ivan.vasko@ssl.berkeley.edu

ABSTRACT

Current sheets with strong transverse (cross field) currents are commonly observed in planetary magnetospheres and serve as a natural energy source for magnetic reconnection. As the most investigated current sheet, the current sheet in the Earth's magnetotail forms in a high-β plasma, with hot ions dominantly contributing to the diamagnetic currents. Spacecraft observations have shown, however, that a superthin electron dominated current sheet can be embedded in the Earth's magnetotail current sheet. In this paper, we develop a model of such superthin current sheets with strong currents produced by anisotropic electrons. We also compare the model with spacecraft observations, which shows reasonable agreement in spatial profiles and magnitudes of the current density. The spatial scale (thickness) of the superthin current sheet is controlled by the equatorial magnetic field component, whereas the current density magnitude is controlled by the electron fire-hose parameter at the equator. Although the current density peak within the superthin current sheet can significantly exceed the background (embedding) current density, the magnetic field magnitude at the superthin current sheet boundary does not exceed 10% of the total magnetic field magnitude. These superthin current sheets are sub-ion (or even electron-scale) structures, which are not sufficiently large/intense to perturb ion dynamics. We discuss applications of the proposed model for the analysis of plasma instabilities in superthin electron-dominated current sheets.

I. INTRODUCTION

The Earth's magnetotail is a high-β region where strong electric currents support self-consistent magnetic fields.[18,58,66] The intensity and spatial distribution of these currents control the magnetotail stability[74,80,94] and determine the efficiency of charged particle acceleration during magnetic reconnection.[41] Multiple spacecraft missions[1,24,39] probing the Earth's magnetotail have provided detailed information about the current sheet, which allows for the development and verification of current sheet models.[79,81,95,96] These models can be further used for the analysis of current sheet dynamics in solar wind,[30,31,63] solar corona,[65,82] and planetary magnetotails.[4,15,19,32,69]

The magnetotail plasma is characterized by hot ions (mostly protons) with a pressure p_i well exceeding the electron pressure, $p_i/p_e \sim 5$ (see Refs. 8 and 89). Thus, diamagnetic currents $\sim c\mathbf{B} \times \nabla p/B^2$ are dominated by ions, and properties of the ion population mainly control the current sheet configuration.[12,81,91,99] Formation of thin current sheets is associated with strong polarization electric fields,[47,77] **E**. Although $\mathbf{E}\times\mathbf{B}$ drift redistributes ion and electron currents and supports strong electron currents at the expense of ion diamagnetic currents,[21,56,57,76] the configuration of such polarized (with $\mathbf{E} \neq 0$) thin current sheets is controlled by ions, and the current sheet thickness is on the ion kinetic scale.[12,13,70,71]

In the high-β magnetotail plasma, ion anisotropy is well constrained by efficient pitch-angle scattering due to magnetic field line curvature,[25,98] as well as a competition between field-aligned cold ionospheric ions and hot transversely accelerated transient ions.[7,91] These lead to a low level of ion temperature anisotropy (see the discussion in Ref. 64).

Unlike ions, the magnetotail electrons are generally anisotropic with the field-aligned pressure $p_{e\|}$ exceeding the transverse pressure $p_{e\perp}$ (see Refs. 16 and 88). Although electron anisotropy is not large (typical $p_{e\|}/p_{e\perp} \in [1.05, 1.2]$), the large electron $\beta_e = 8\pi p_{e\perp}/B^2 > 10$ provides strong electron anisotropic currents with a relative magnitude (compared to the total current) of $\sim\beta_e(p_{e\|}/p_{e\perp} - 1)$.[6,11] In contrast to ion currents on a spatial scale of thermal ion gyroradius,[66,71] electron currents have their own spatial scale that can be significantly smaller than the ion gyroradius.[44,97] These electron currents form superthin current sheets[14,60,61] embedded into the ion-scale current sheets. The strongest electron current sheets are formed by anisotropic electrons around the magnetic reconnection region,[35,51,52] where anisotropy is self-consistently supported by electron trapping and acceleration by polarization electric fields.[33,37] Away from the reconnection region, the anisotropic electron population can be formed by field-aligned outflow of ionospheric electrons.[87]

Properties of the superthin current sheets, as supported by anisotropic electrons, significantly differ from properties of classical current sheets supported by diamagnetic currents. Due to the sub-ion scale of superthin current sheets, ion motion is not perturbed by magnetic field variations within these current sheets. Thus, these current sheets may be a source for electron-dominated instabilities[45,46,53] and electron-dominated magnetic reconnection.[67] Moreover, electron anisotropic currents in the magnetotail are often associated with field-aligned currents observed within reconnection regions[2,35,51] and in thin current sheets.[5,90] Investigation of these sub-ion scale current sheet instabilities and reconnection requires realistic superthin current sheet models with strong currents carried by anisotropic electrons. This study aims to develop such a model. We use the observed electron distribution function to determine the equation of state and the current density of anisotropic electrons. The electron-dominated current sheet is embedded into the background diamagnetic current (produced predominantly by ions), with a self-consistent magnetic field configuration. To verify this model, we use MMS observations[24] of superthin current sheets in the Earth's magnetotail.

II. ELECTRON EQUATION OF STATE

A crucial element of current sheet models is the equation of state that is used to describe the relation between plasma pressure components and magnetic field, $p_{e\|}, p_{e\perp} = p_{e\|}(\mathbf{B}), p_{e\perp}(\mathbf{B})$. For 2D and 1D current sheet configurations (current density is along y, the strongest spatial gradient is along z, the reversing magnetic field component is $B_x(z)$, and the magnetic field component $B_z \ll \max|B_x|$), there are two classical examples of such equations of state. For an Maxwellian plasma drifting along y, the pressure can be written as $p \sim \exp(-A_y/A_0)$ with $A_y(x, z)$ being the vector potential component[20,22,73,75] ($\mathbf{B} = \nabla \times \mathbf{e}_y A_y$); for an anisotropic Maxwellian plasma with the following velocity distribution

$$f(\mathbf{v}) = const \cdot \exp\left(-\frac{mv_{0\|}^2}{2T_{0\|}} - \frac{mv_{0\perp}^2}{2T_{0\perp}}\right), \tag{1}$$

equation of states are[29,92]

$$\begin{aligned} p_{e\|} &= n_0 T_{\|0} \\ p_{e\perp} &= n_0 T_{\perp 0} \end{aligned} \quad \begin{aligned} &\left[\frac{B}{B_{eq}(1-r)+Br}\right] \\ &\left[\frac{B}{B_{eq}(1-r)+Br}\right]^2 \end{aligned}, \tag{2}$$

where $B = |\mathbf{B}|$, $T_{0\|,\perp}$ are plasma temperatures at the equatorial plane $z = 0$ (where $B_x = 0$ and $B = B_{eq} = B_z$), $v_{0\|,\perp}$ are velocity components at $z = 0$, $r = T_{0\perp}/T_{0\|}$. These equations of state describe non-polarized plasma ($\mathbf{E} = 0$) and are widely used in constructing current sheet models.[44,54,100] Equations (2) describe pressure components for anisotropic Maxwellian plasma trapped within the current sheet, i.e., all particle trajectories can be integrated, by conserving energy $m_e(v_\|^2 + v_\perp^2)/2$ and magnetic moment $m_e v_\perp^2/2B$, to calculate the velocity distribution for any given B along magnetic field lines. This distinguishes Eq. (2) from the equations of state on transient electrons crossing the current sheet from one boundary (with $B_x > 0$) to another boundary (with $B_x < 0$); see examples of such equations of state in Refs. 35 and 97.

We aim to generalize Eq. (2) for a realistic electron distribution in the magnetotail current sheet,[16,86]

$$\begin{aligned} f(\mathbf{v}) = C&\left(1 + \frac{1}{\kappa}\left(\frac{mv_{0\|}^2}{2T_{0\|}} + \frac{mv_{0\perp}^2}{2T_{0\perp}} - \frac{e\varphi}{T_{0\|}}\right)\right)^{-1-\kappa} \\ &\times\exp\left(-\frac{mv_{0\|}^2}{2T_{0\|}} - \frac{mv_{0\perp}^2}{2T_{0\perp}} + \frac{e\varphi}{T_{0\|}}\right), \end{aligned} \tag{3}$$

where $\kappa \in [0, 1]$, and φ is the scalar potential at the equatorial plane (φ can be set zero at the equator, but off-equator φ is nonzero in polarized current sheets with $\mathbf{E} \neq 0$). Using Liouville's theorem, we recalculate this distribution function at any position (any B) along magnetic field lines,

$$\begin{aligned} f = C&\left(1 + \frac{1}{\kappa}\left(\frac{mv_\|^2}{2T_{0\|}} + \frac{mv_\perp^2}{2T_{0\perp}}\left(\frac{(1-r)+rb}{b}\right) - \Phi\right)\right)^{-1-\kappa} \\ &\times\exp\left(-\frac{mv_\|^2}{2T_{0\|}} - \frac{mv_\perp^2}{2T_{0\perp}}\left(\frac{(1-r)+rb}{b}\right) + \Phi\right), \end{aligned} \tag{4}$$

where $b = B/B_{eq}$ is the magnetic field in units of its equatorial magnetic field magnitude and $\Phi = e\varphi/T_{0\|}$. Figure 1 shows that electron anisotropy decreases with b and distribution (4) tends to be isotropic far from the equatorial plane.

Using Eq. (4), we calculate electron density $n_e(B, B_{eq}, \Phi)$ and pressure components $p_{e\|,\perp}(B, B_{eq}, \Phi)$. For an arbitrary κ, there are no analytical expressions for $n_e(B, B_{eq}, \Phi)$ and $p_{e\|,\perp}(B, B_{eq}, \Phi)$; thus we numerically integrate Eq. (4). Note that the main differences between pressure components given by Eq. (2) and components obtained from integrating Eq. (4) are: the exponential factor $\sim e^{-\Phi}$ and power-law distribution of low-energy particles. Equation (2) has been written for an electroneutral plasma, and in a more general case, the factor $\sim e^{-\Phi}$ should be added to these equations. Contribution of low-energy

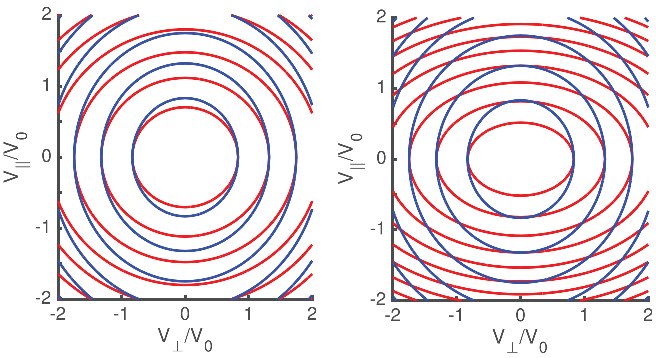

FIG. 1. Distribution function (4) for two values of equatorial anisotropy: $r = 2/3$ (left), $r = 1/3$ (right). Blue curves show equatorial electron distributions and red curves show electron distributions at $b = B/B_{eq} = 5$. Velocity components are normalized to the equatorial thermal velocity $v_0 = \sqrt{2T_{0\|}/m}$.

particles to the pressure component is not significant, but the factor $\sim(1-\Phi/\kappa)^{-1-\kappa}$ can be large (see Φ profiles below). Thus, although there is no analytical form for the pressure components of distribution function (4), we can speculate that these components mostly differ from Eq. (2) for significantly charged current sheets (i.e., large Φ).

The scalar potential Φ is defined by the quasi-neutrality condition, $n_e = n_i$ for a given ion density. Multiple approaches can be used to introduce n_i, e.g., for isotropic isothermal Maxwellian distribution of ions, $n_i \sim \exp(-A_y/A_0 - e\varphi/T_i)$ (see Refs. 55 and 93); for anisotropic Maxwellian distributions, $n_i \sim \exp(-e\varphi/T_i)N(B, B_{eq})$ (see Refs. 14, 50, and 92); for sophisticated non-gyrotropic ion distributions, $n_i \sim \exp(-e\varphi/T_i)N(A_y/A_0)$ (see Refs. 21, 27, and 76). We are looking for an ion distribution within a superthin current sheet dominated by electron currents, and thus we can assume ions to be demagnetized within these thin current sheets around the equatorial plane, i.e., $n_i \sim \exp(-e\varphi/T_i) = \exp(-\Phi/\tau)$ with $\tau = T_i/T_{0\|}$. The scalar potential Φ is determined from the $n_e(B, B_{eq}, \Phi) - n_0\exp(-\Phi/\tau) = 0$ equation.

Figure 2 shows Φ for different system parameters. Stronger electron anisotropy $1/r$ and larger τ result in larger $|\Phi|$, which reaches

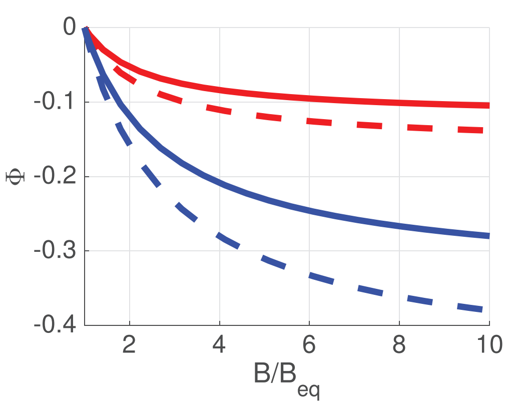

FIG. 2. Distribution of scalar potential $\Phi = e\varphi/T_{0\|}$ along magnetic field lines for different system parameters: $k = 1/2$, $\tau = 1$ (solid) and $\tau = 5$ (dashed), $r = 2/3$ (red) and $r = 1/3$ (blue).

$\sim$30% of the electron temperature. The potential is negative and decreases away from the equatorial plane with $\partial\Phi/\partial B < 0$, i.e., the field-aligned electric field $E_\| \sim -\partial\Phi/\partial B$ is directed away from the equator and should confine electrons within the current sheet. This spatial distribution of $E_\|$ is typical for both thin current sheets[14] and current sheets around the reconnection region.[33,34,42]

Substituting the scalar potential Φ into the pressure component equations, $p_{e\|}$ and $p_{e\perp}$, we plot the equation of state $p_{e\|,\perp}(B)$ in Fig. 3. Both parallel and transverse pressure components grow along magnetic field lines, as expected for the field-aligned anisotropy $1/r < 1$ (more energetic electrons have smaller pitch angles and elongated bounce orbits).

The pressure components determine the parameter of the electron fire-hose instability, which plays a crucial role in models of electron current,[14]

$$\Lambda = 4\pi\frac{p_{e\|}(B) - p_{e\perp}(B)}{B^2} = \frac{\beta_{eq}}{2}\frac{p_{e\perp}(B)}{b^2 p_{e\perp,eq}}\left(\frac{p_{e\|}}{p_{e\perp}} - 1\right), \tag{5}$$

where $\beta_{e,eq}$ is the ratio of electron thermal and magnetic pressures at the equator. The maximum value of Λ is $\Lambda_{B_x=0} = \beta_{eq}(1/r - 1)/2$. The spatial localization of Λ leads to a localization of the anisotropic electron currents. Figure 4 shows that Λ does not depend on τ, i.e., the electrostatic potential barely affects the $p_{e\|}/p_{e\perp}$ ratio. The parameter κ of the velocity distribution (4) controls the low-energy part of the distribution and does not alter the pressure components dominated by hot electrons. Λ drops to zero for $B/B_{eq} > 3$, and thus the current density of anisotropic electrons is expected to be strongly localized around the equatorial plane.

III. EMBEDDED CURRENT SHEET MODEL

To incorporate anisotropic electron currents into the current sheet model, we use the ambient (ion and electron) diamagnetic currents given by the Harris[43] model $j_{bg} = j_0\cosh^2(z/L)$ or 2D generalizations of that model.[54,73,100] Background current density j_0 and current sheet thickness L determine the magnetic field magnitude $B_0 = 4\pi j_0 L/c$. The electron superthin current sheet with the current (see a review in Refs. 14, 48, 64, and 78)

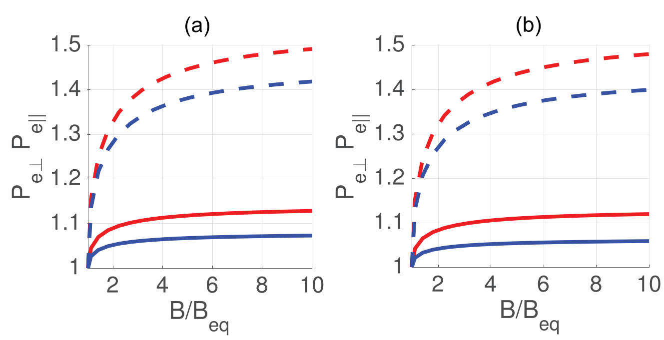

FIG. 3. Profiles of electron pressure components $p_{e\|}$) (solid) and $p_{e\perp}$(dashed) along B for model (4). All pressure components are normalized to equatorial values. Parameters are: (a) $k = 1/2$, $r = 2/3$, $\tau = 1$ (red), and $\tau = 5$ (blue); (b) $k = 1$, $r = 2/3$, $\tau = 1$ (red), and $\tau = 5$ (blue).

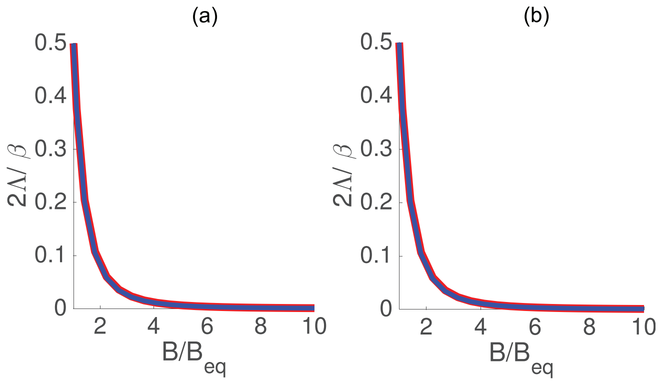

FIG. 4. Profiles of $2\Lambda(B)/\beta_{eq}$ for different system parameters: (left) $2\Lambda/\beta$ for $k = 1/2$, $r = 2/3$, $\tau = 1$ (red and $\tau = 5$ (blue); (right) $2\Lambda/\beta$ for $k = 1$, $r = 2/3$, $\tau = 1$ (red), and $\tau = 5$ (blue).

$$\mathbf{j}_{e,ani} = c\frac{p_{e\parallel} - p_{e\perp}}{B^2}\frac{\mathbf{B}\times(\mathbf{B}\nabla)\mathbf{B}}{B^2} \approx \frac{cp_{e\perp}}{B^2}\left(\frac{p_{e\parallel}}{p_{e\perp}} - 1\right)\frac{\partial B_x}{\partial z}\mathbf{e}_y$$
$$= \frac{\beta_{eq}}{2}\frac{cp_{e\perp}}{4\pi p_{e\perp,eq}}\left(\frac{p_\parallel}{p_\perp} - 1\right)\frac{\partial B_x}{\partial z}\mathbf{e}_y \qquad (6)$$

is embedded into the j_{bg} profile. Due to the small thickness of electron current sheet, the magnetic field variation supported by electron currents does not perturb ion motion and j_{bg} remains unchanged. Moreover, on the spatial scale of the superthin electron current sheet, $B_z = B_{eq}$ field can be assumed to be constant (see a schematic of this model in Fig. 5).

In such a quasi-1D configuration, the current density $j_y \approx (c/4\pi)\partial B_x/\partial z$ and $j_{e,ani} = \Lambda j_y$, where Λ is given by Eq. (5). Combing j_{bg} and $j_{e,ani}$, we can write $j_y = j_{bg} + \Lambda j_y$ and

$$\frac{\partial B_x(z)}{\partial z} = \frac{4\pi}{c}\frac{j_{bg}(z)}{1 - \Lambda(B(z))}, \qquad (7)$$

where $B = \sqrt{B_x^2(z) + B_{eq}^2}$. The solution of Eq. (7) provides the self-consistent magnetic field $B_x(z)$ that coincides with Harris solution $[B_x = B_0\tanh(z/L)]$ for isotropic plasmas with $\Lambda = 0$. Note that Eq. (7) omits the diamagnetic contribution of the anisotropic electron

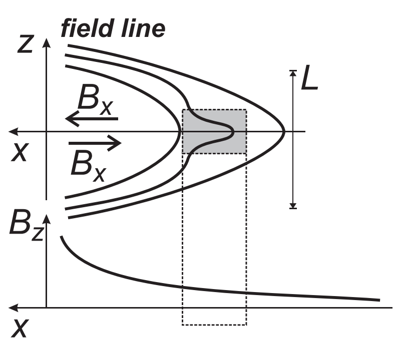

FIG. 5. Schematic of the supper-thin current sheet embedded into the 2D magnetotail current sheet. The gray region shows the superthin current sheet with small spatial scale along the magnetotail (along x). There is no strong variation of B_z over the spatial scale of the superthin current sheet, and thus we assume $B_z = const$.

population (for a more general form of this equation see Refs. 48 and 64). This simplification is justified by the smallness of the temperature (small diamagnetic currents) of the anisotropic electrons.[16]

Figure 6 shows profiles of $j_y \approx (c/4\pi)\partial B_x/\partial z$ with self-consistent B_x from Eq. (7). The anisotropic electrons provide a strong peak of the current density with a spatial scale (thickness) much smaller than the thickness of the ambient current density profile. Electron equatorial β_{eq} and anisotropy $1/r$ play the same role in determining the peak (equatorial) Λ value: increases of β_{eq} and $1/r$ result in increases of the electron current density magnitude. The equatorial magnetic field B_{eq} determines the spatial scale of Λ and thus controls the thickness of the electron current density peak.

IV. SPACECRAFT OBSERVATIONS

To verify the proposed model of superthin, electron-dominated current sheets, we use observations from MMS spacecraft[24] in the Earth's magnetotail. The main advantage of the MMS mission is the unprecedented high-resolution plasma measurements[68] that allow direct calculation of ion and electron currents in the magnetotail current sheet.[56] We utilize the survey mode dataset with 1/16s-resolution magnetic field[72] and 3s-resolution plasma moments (all vectors are in GSM coordinates).

Figures 7–9 show an overview of three current sheet crossings. Panels (a) show B_x reversals across the sheet and relatively small B_z field directed almost across the current sheet surface. All three events are observed during quiet geomagnetic conditions, i.e., plasma flows are weak with $|v_x| < 100$ km/s [see panels (b)]. We focus on the current sheet crossings with small B_x variations (<10 nT) and almost flat density profiles [see panels (b)]. Such flat density profiles are typical for these so-called embedded current sheets that are characterized by intense currents embedded into a broad plasma sheet.[9,71]

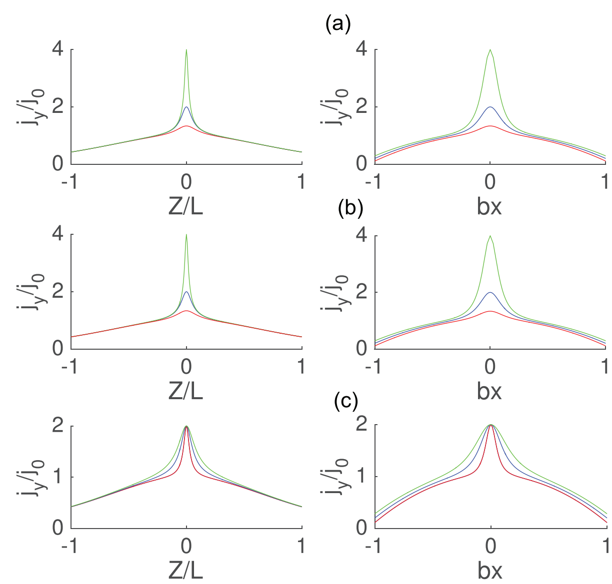

FIG. 6. Solutions of Eq. (7) for different system parameters: (a) $B_z/B_0 = 0.2$, $1/r = 1.1$, and $\beta = 5$ (red), $\beta = 10$ (green); $\beta = 15$ (blue); (b) $B_z/B_0 = 0.2$, $\beta = 10$, and $1/r = 1.05$ (red), $1/r = 1.1$ (green), $1/r = 1.15$ (blue); (c) $1/r = 1.1$, $\beta = 10$, and $B_z/B_0 = 0.1$ (red), $B_z/B_0 = 0.2$ (green), and $B_z/B_0 = 0.3$ (blue).

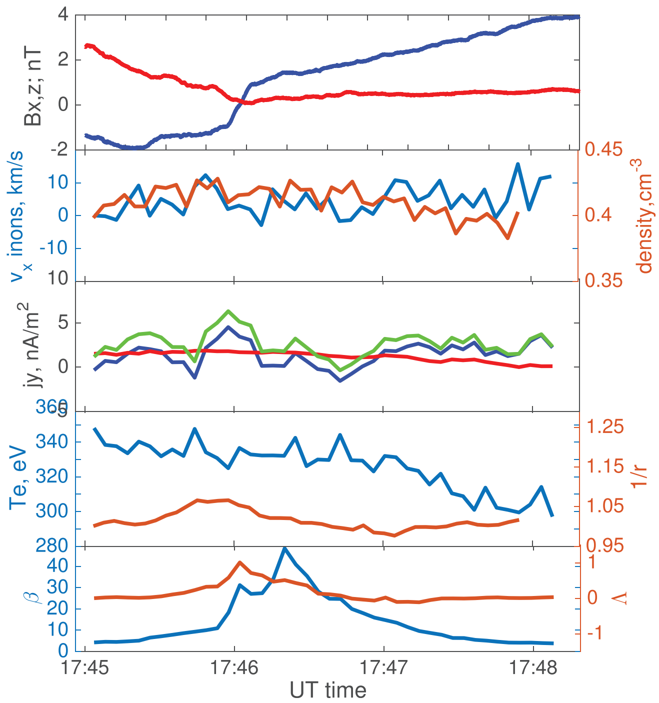

FIG. 7. The current sheet crossed by MMS spacecraft on 2017-08-15. Panel (a) shows B_x and B_z magnetic field components in GSM coordinates. Panel (b) shows ion plasma flow and plasma density. Panel (c) shows ion (red), electron (blue), and total (green) current densities. Panel (d) shows electron temperature and electron anisotropy $T_{\|}/T_{\perp} = 1/r$. Panel (e) shows electron β and fire-hose parameter.

All three current sheets contain a strong peak of electron currents around the B_x reversal and very weak ion currents [see panels (c)]. Therefore, these current sheets satisfy our criteria of the electron sheet embedded into a much weaker ion sheet. (Note that the observed ion current density magnitude can be reduced due to current sheet polarization[57]) The spatial scales of the electron current sheets are about $\sim c\Delta B_x/4\pi j_y \sim 250-500$ km for magnetic field variation $\Delta B_x \sim 5$ nT and current density peak $\sim$15 nA/m^2. This scale is smaller than the typical current sheet scale, $\sim$1000 − 3000 km (see Ref. 66), i.e., we indeed deal with thin electron current sheets embedded into a thicker ion sheet.

All three current sheets are characterized by a weak electron temperature variation, with evident electron anisotropy $T_{\|}/T_{\perp} = 1/r \sim 1.1$ [see panels (d)]. This is the typical electron anisotropy level in the Earth's magnetotail.[16] Due to small B_z, the electron β_e reaches $10-30$ around the B_x reversal [see panels (e)]. This large β_e leads to large magnitudes of the fire-hose parameter $[\Lambda = (\beta_{eq}/2)(1/r-1)]$ around the B_x reversal: Λ reaches $0.5-1$, which is larger than typical Λ values for the magnetotail current sheets.[6] Therefore, in these current sheets, anisotropic electrons should contribute significantly to the current density generation and may explain the observed peaks of the electron current density.

Figure 10 shows a comparison of model current density profiles (i.e., the solution of Eq. (7) with β_{eq}, $1/r$, and B_0 directly from observations) and observed profiles during the three events from Figs. 7 and 8. For j_0, we use the current density observed at the boundary of observed current sheets. Parameters β_{eq}, $1/r$ are averaged over the range of $|B_x| < 1$ nT from observations. A comparison of the model and observed current density profiles demonstrate that Eq. (7) correctly reproduces the main features of the superthin electron current sheet embedded into an ion-scale sheet. Both the observed scale (i.e., B_x range) and current density magnitude are well modeled.

Figure 10 compares the model and observed current density profiles, but this comparison only verifies basic model properties. Verification of sophisticated model characteristics, such as polarization

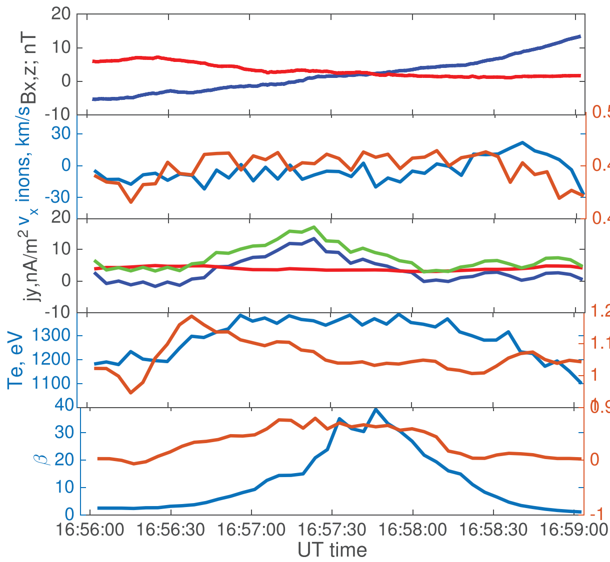

FIG. 8. Same as in Fig. 7, but for the current sheet crossed by MMS spacecraft on 2017-08-18.

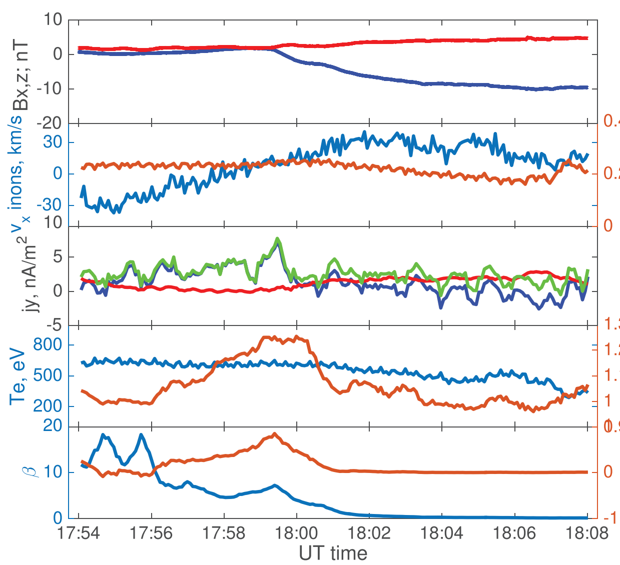

FIG. 9. Same as in Fig. 7, but for the current sheet crossed by MMS spacecraft on 2017-08-26.

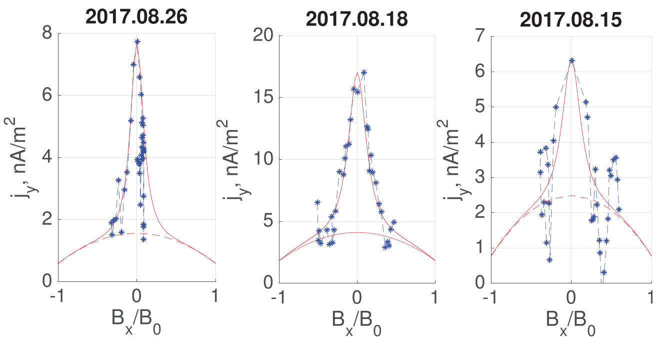

FIG. 10. Comparison of observed current density profiles for events shown in Figs. 7–9 (blue) and model profiles from Eq. (7) with input parameters from observations (red solid). Profiles for an isotropic model ($r = 1$) are shown by dashed red curves.

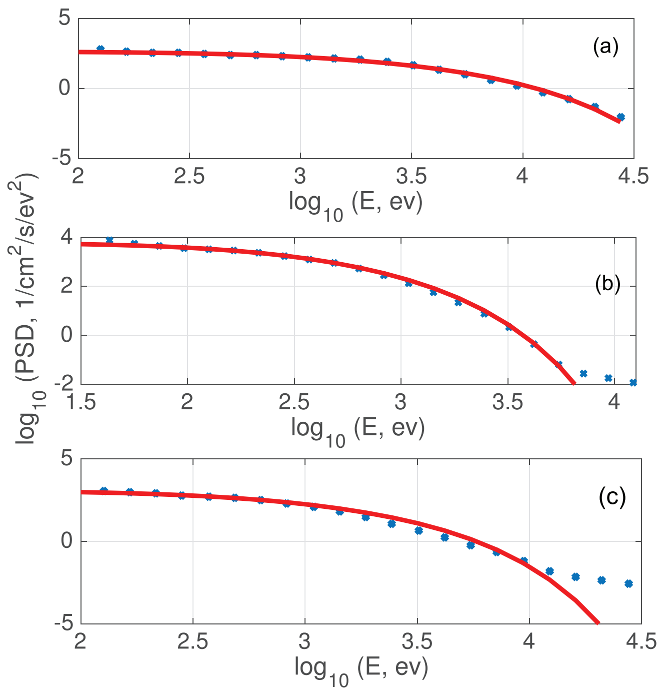

FIG. 11. Comparison of electron phase space density f measured by MMS (blue dots) and modeled as $f \sim (1 + E/E_0\kappa)^{-\kappa-1} \exp(-E/E_0)$ (red curves) (a) during the event from Fig. 7, with fitting parameters $\kappa = 1/2$, $E_0 = 3.7$ keV; (b) during the event from Fig. 8, with fitting parameters $\kappa = 1/2$, $E_0 = 0.7$ keV; (c) during the event from Fig. 9, with fitting parameters $\kappa = 1/2$, $E_0 = 1.5$ keV.

electric field distributions and electron energy spectra, is more complicated. Although spacecraft observations[2] and numerical simulations[35,51] of anisotropic electrons in the reconnected current sheets demonstrate the presence of a strong polarization electric fields, such fields are expected to be much weaker in the quasi-stationary current sheets shown in Figs. 7–9. Thus, we cannot compare observational and model distributions of electric fields. Equation (4) fits observed electron energy spectra,[16] and these spectra can be compared with observations around the equatorial plane (but observations do not provide the spectrum evolution along magnetic field lines, and thus we cannot compare electron flux anisotropy as a function of B/B_{eq}). Figure 11 shows that for events from Figs. 7–9, the main part of observed electron spectra is well fitted by Eq. (4) with reasonable κ values. There is also a high-energy electron population that cannot be fitted by the two-component model given by Eq. (4), but this component does not contribute significantly to the phase space density.

V. DISCUSSION AND CONCLUSION

In this study, we have investigated very intense superthin (subion scale) current sheets that are generated by anisotropic electrons observed in the Earth's magnetotail. Although the current density magnitude within these superthin current sheets can be very large (e.g., the three examples shown in Fig. 10 exhibit $j_y \sim 10 - 20$ nA/m^2, higher than currents in thin ion-scale current sheets, see Refs. 10 and 70), the magnetic field variation B_x across the current density peak is quite small (and would be even smaller if negative diamagnetic currents of parallel anisotropic electrons would be taken into account). Indeed, Fig. 6 shows that even the most anisotropic (larger $1/r$ or equivalently larger β_{eq}) current sheets with the largest thickness (larger B_{eq}/B_0) are bounded by $B_x \sim 10\%$ of the total magnetic field variation. This justifies our hypothesis that a superthin electron current sheet does not disturb ion dynamics, and thus would not alter the background current density profile.

To construct the superthin current sheet model, we use anisotropic electron MHD, which is applicable for magnetized plasma, but not for unmagnetized systems.[17] Therefore, an important question for the constructed model is the electron magnetization. Indeed, the superthin current sheet provides a small-scale magnetic field variation that can scatter electrons and result in their demagnetization.[28,62] To check the applicability of anisotropic MHD, we estimate the adiabaticity parameter $\kappa = \sqrt{R_c/\rho_e}$, the ratio of the magnetic field line curvature radius and electron gyroradius at the equator (see Refs. 23, 36, and 98). For $\kappa \sim 1$ electrons become demagnetized, and for $\kappa \gg 1$ MHD is applicable. In 1D current sheets, the magnetic field-line curvature radius is $R_c \approx (B_{eq}\tilde{L}/\tilde{B}_0)$, where $\tilde{B}_0 \le B_0/10$ is the magnetic field magnitude at the superthin current sheet boundary, and $\tilde{L} = \tilde{B}_0 c/4\pi j_y$ is the superthin current sheet thickness. The electron gyroradius at the equator is $\rho_e = v_0 m_e c/eB_{eq}$, with v_0 being the electron thermal speed. Substituting ρ_e and R_c into κ, we get $\kappa = \sqrt{B_{eq}^2 e/4\pi j_y v_0 m_e} = \sqrt{2j^*/j_y\beta_{eq}}$, with $j^* = ev_0 n_0$ the current of demagnetized electrons. Although the observed current density j_y can reach j^* in the most intense current sheets around the reconnection region,[38,85] j_y is typically much smaller than j^* and can approach $j^*\sqrt{T_i m_e/T_{0\perp} m_i} \sim j^*/20$ for intense currents.[11] Taking into account that $j_y/j^* \sim 1/20$ and $\beta_{eq} \sim 10 - 40$, we obtain $\kappa \ge 1$, i.e., electrons are mostly magnetized within superthin current sheets and we can describe electron currents using the anisotropic MHD. However, for the most intense current sheets with large β_{eq}, the applicability of MHD becomes questionable and effects of electron demagnetization should be taken into account.

Strong electron currents and strong electron anisotropy are free energy sources for plasma instabilities. First of all, the electron firehose instability can develop in the electron plasma with $\Lambda \ge 1$ (the resonant electron fires-hose instability tends to have a lower Λ

threshold[40,45]). This instability generates nonpropagating small-scale waves that can convert to whistler and electron cyclotron waves.[26,45] Electron scattering by these waves constrains the electron anisotropy and prevent $\Lambda > 1$, or even smaller Λ for resonant fire-hose mode.[40] Therefore, we speculate that formation and dynamics of superthin current sheets should be associated with electron-scale waves due to instability of the electron distribution. Moreover, the Alfvén speed drops to zero for $\Lambda \sim 1$ (see Ref. 49), and the superthin current sheet can be treated as nonlinear very oblique Alfvén wave (that does not propagate due to $\Lambda \sim 1$) or as a rotation discontinuity resulted from Alfvén wave steepening.[59] These superthin current sheets are elements of nonlinear Alfvenic turbulence,[83,84] and investigation of their configuration and stability contributes to models of turbulence development and saturation in anisotropic plasma.

To conclude, we have proposed a model of the superthin current sheet supported by strong currents of anisotropic electrons. This model takes into account realistic electron velocity distributions in the Earth's magnetotail. Embedded into a thick, low-intensity ion current sheet, the modeled superthin current sheet reproduces the current density distribution from MMS observations of highly anisotropic electrons. Validation with spacecraft observations demonstrates that this model can be used for further investigations of the current sheet stability and generation of electron-scale waves in the Earth's magnetotail.

ACKNOWLEDGMENTS

The work of S.R.K., E.V.Y., and A.S.L. was supported by the Russian Scientific Foundation, Project No. 19–12-00313. The work of A.V.A. and I.Y.V. was supported by NSF Project No. 1902699.

DATA AVAILABILITY

The data for figures of this study are available from the corresponding author upon reasonable request, whereas spacecraft data (MMS FGM and FPI measurements) are available in open database https://lasp.colorado.edu/mms/sdc/public/datasets/. Data access and processing was done using SPEDAS V3.1.[3]

REFERENCES

1. V. Angelopoulos, Space Sci. Rev. **141**, 5–34 (2008).
2. V. Angelopoulos, A. Artemyev, T. D. Phan, and Y. Miyashita, Nat. Phys. **16**(3), 317–321 (2020).
3. V. Angelopoulos, P. Cruce, A. Drozdov, E. W. Grimes, N. Hatzigeorgiu, D. A. King, D. Larson, J. W. Lewis, J. M. McTiernan, D. A. Roberts, C. L. Russell, T. Hori, Y. Kasahara, A. Kumamoto, A. Matsuoka, Y. Miyashita, Y. Miyoshi, I. Shinohara, M. Teramoto, J. B. Faden, A. J. Halford, M. McCarthy, R. M. Millan, J. G. Sample, D. M. Smith, L. A. Woodger, A. Masson, A. A. Narock, K. Asamura, T. F. Chang, C.-Y. Chiang, Y. Kazama, K. Keika, S. Matsuda, T. Segawa, K. Seki, M. Shoji, S. W. Y. Tam, N. Umemura, B.-J. Wang, S.-Y. Wang, R. Redmon, J. V. Rodriguez, H. J. Singer, J. Vandegriff, S. Abe, M. Nose, A. Shinbori, Y.-M. Tanaka, S. UeNo, L. Andersson, P. Dunn, C. Fowler, J. S. Halekas, T. Hara, Y. Harada, C. O. Lee, R. Lillis, D. L. Mitchell, M. R. Argall, K. Bromund, J. L. Burch, I. J. Cohen, M. Galloy, B. Giles, A. N. Jaynes, O. Le Contel, M. Oka, T. D. Phan, B. M. Walsh, J. Westlake, F. D. Wilder, S. D. Bale, R. Livi, M. Pulupa, P. Whittlesey, A. DeWolfe, B. Harter, E. Lucas, U. Auster, J. W. Bonnell, C. M. Cully, E. Donovan, R. E. Ergun, H. U. Frey, B. Jackel, A. Keiling, H. Korth, J. P. McFadden, Y. Nishimura, F. Plaschke, P. Robert, D. L. Turner, J. M. Weygand, R. M. Candey, R. C. Johnson, T. Kovalick, M. H. Liu, R. E. McGuire, A. Breneman, K. Kersten, and P. Schroeder, Space Sci. Rev. **215**, 9 (2019).
4. A. V. Artemyev, V. Angelopoulos, J. S. Halekas, A. Runov, L. M. Zelenyi, and J. P. McFadden, J. Geophys. Res. **122**, 5404–5417, https://doi.org/10.1002/2017JA024078 (2017).
5. A. V. Artemyev, V. Angelopoulos, J. Liu, and A. Runov, Geophys. Res. Lett. **44**, 5–11, https://doi.org/10.1002/2016GL072011 (2017).
6. A. V. Artemyev, V. Angelopoulos, I. Y. Vasko, A. A. Petrukovich, A. Runov, Y. Saito, L. A. Avanov, B. L. Giles, C. T. Russell, and R. J. Strangeway, J. Geophys. Res. **125**(1), e2019JA027251 (2020).
7. A. V. Artemyev, V. Angelopoulos, I. Y. Vasko, X. J. Zhang, A. Runov, and L. M. Zelenyi, J. Geophys. Res. **124**(5), 3454–3467, https://doi.org/10.1029/2019JA026604 (2019).
8. A. V. Artemyev, W. Baumjohann, A. A. Petrukovich, R. Nakamura, I. Dandouras, and A. Fazakerley, Ann. Geophys. **29**, 2253–2257 (2011).
9. A. V. Artemyev, A. A. Petrukovich, R. Nakamura, and L. M. Zelenyi, J. Geophys. Res. **115**, A12255, https://doi.org/10.1029/2010JA015702 (2010).
10. A. V. Artemyev, A. A. Petrukovich, R. Nakamura, and L. M. Zelenyi, J. Geophys. Res. **116**, A09233, https://doi.org/10.1029/2011JA016801 (2011).
11. A. V. Artemyev, A. A. Petrukovich, R. Nakamura, and L. M. Zelenyi, J. Geophys. Res. **120**, 3804–3820, https://doi.org/10.1002/2015JA021046 (2015).
12. A. V. Artemyev, A. A. Petrukovich, L. M. Zelenyi, H. V. Malova, V. Y. Popov, R. Nakamura, A. Runov, and S. Apatenkov, Ann. Geophys. **26**, 2749–2758 (2008).
13. A. V. Artemyev, A. A. Petrukovich, L. M. Zelenyi, R. Nakamura, H. V. Malova, and V. Y. Popov, Ann. Geophys. **27**, 4075–4087 (2009).
14. A. V. Artemyev, I. Y. Vasko, V. Angelopoulos, and A. Runov, Phys. Plasmas **23**(9), 092901 (2016).
15. A. V. Artemyev, I. Y. Vasko, and S. Kasahara, Planet. Space Sci. **96**, 133–145 (2014).
16. A. V. Artemyev, A. P. Walsh, A. A. Petrukovich, W. Baumjohann, R. Nakamura, and A. N. Fazakerley, J. Geophys. Res. **119**, 7214–7227, https://doi.org/10.1002/2014JA020350 (2014).
17. M. Ashour-Abdalla, L. M. Zelenyi, V. Peroomian, and R. L. Richard, J. Geophys. Res. **99**, 14891–14916, https://doi.org/10.1029/94JA00141 (1994).
18. W. Baumjohann, A. Roux, O. Le Contel, R. Nakamura, J. Birn, M. Hoshino, A. T. Y. Lui, C. J. Owen, J. Sauvaud, A. Vaivads, D. Fontaine, and A. Runov, Ann. Geophys. **25**, 1365–1389 (2007).
19. K. W. Behannon, L. F. Burlaga, and N. F. Ness, J. Geophys. Res. **86**, 8385–8401, https://doi.org/10.1029/JA086iA10p08385 (1981).
20. J. Birn, J. Geophys. Res. **84**, 5143–5152, https://doi.org/10.1029/JA084iA09p05143 (1979).
21. J. Birn, K. Schindler, and M. Hesse, J. Geophys. Res. **109**, 2217, https://doi.org/10.1029/2003JA010303 (2004).
22. J. Birn, R. R. Sommer, and K. Schindler, J. Geophys. Res. **82**, 147–154, https://doi.org/10.1029/JA082i001p00147 (1977).
23. J. Büchner and L. M. Zelenyi, J. Geophys. Res. **94**, 11821–11842, https://doi.org/10.1029/JA094iA09p11821 (1989).
24. J. L. Burch, T. E. Moore, R. B. Torbert, and B. L. Giles, Space Sci. Rev. **199**, 5–21 (2016).
25. G. R. Burkhart, P. B. Dusenbery, and T. W. Speiser, J. Geophys. Res. **100**, 107–118, https://doi.org/10.1029/94JA02221 (1995).
26. E. Camporeale and D. Burgess, J. Geophys. Res. **113**, A07107, https://doi.org/10.1029/2008JA013043 (2008).
27. E. Camporeale and G. Lapenta, J. Geophys. Res. **110**, A07206, https://doi.org/10.1029/2004JA010779 (2005).
28. B. V. Chirikov, *Particle Dynamics in Magnetic Traps*, 1st ed. (Consultants Bureau, New York, 1987), Vol. 13.
29. S. W. H. Cowley, Planet. Space Sci. **26**, 1037–1061 (1978).
30. J. de Keyser, M. Roth, J. Lemaire, B. T. Tsurutani, C. M. Ho, and C. M. Hammond, Sol. Phys. **166**(2), 415–422 (1996).
31. J. de Keyser, M. Roth, B. T. Tsurutani, C. M. Ho, and J. L. Phillips, Astron. Astrophys. **321**, 945–959 (1997).
32. G. A. DiBraccio, J. R. Espley, J. R. Gruesbeck, J. E. P. Connerney, D. A. Brain, J. S. Halekas, D. L. Mitchell, J. P. McFadden, Y. Harada, R. Livi, G. Collinson, T. Hara, C. Mazelle, and B. M. Jakosky, Geophys. Res. Lett. **42**, 8828–8837, https://doi.org/10.1002/2015GL065248 (2015).
33. J. Egedal, W. Daughton, and A. Le, Nat. Phys. **8**, 321–324 (2012).

[34] J. Egedal, W. Daughton, A. Le, and A. L. Borg, Phys. Plasmas **22**(10), 101208 (2015).
[35] J. Egedal, A. Le, and W. Daughton, Phys. Plasmas **20**(6), 061201 (2013).
[36] J. Egedal, A. Le, W. Daughton, B. Wetherton, P. A. Cassak, J. L. Burch, B. Lavraud, J. Dorelli, D. J. Gershman, and L. A. Avanov, Phys. Rev. Lett. **120**(5), 055101 (2018).
[37] J. Egedal, A. Lê, N. Katz, L.-J. Chen, B. Lefebvre, W. Daughton, and A. Fazakerley, J. Geophys. Res. **115**, A03214, https://doi.org/10.1029/2009JA014650 (2010).
[38] J. Egedal, J. Ng, A. Le, W. Daughton, B. Wetherton, J. Dorelli, D. Gershman, and A. Rager, Phys. Rev. Lett. **123**(22), 225101 (2019).
[39] C. P. Escoubet, M. Fehringer, and M. Goldstein, Ann. Geophys. **19**, 1197–1200 (2001).
[40] S. P. Gary and K. Nishimura, Phys. Plasmas **10**, 3571–3576 (2003).
[41] W. Gonzalez and E. Parker, *Magnetic Reconnection* (Springer International Publishing, Zürich, Switzerland, 2016), Vol. 427.
[42] C. C. Haggerty, M. A. Shay, J. F. Drake, T. D. Phan, and C. T. McHugh, Geophys. Res. Lett. **42**, 9657–9665, https://doi.org/10.1002/2015GL065961 (2015).
[43] E. Harris, Nuovo Cimento **23**, 115–123 (1962).
[44] L.-N. Hau, Geophys. Res. Lett. **20**, 555–558, https://doi.org/10.1029/93GL00243 (1993).
[45] P. Hellinger, P. M. Trávníček, V. K. Decyk, and D. Schriver, J. Geophys. Res. **119**, 59–68, https://doi.org/10.1002/2013JA019227 (2014).
[46] P. Hellinger and Š. Štverák, J. Plasma Phys. **84**(4), 905840402 (2018).
[47] M. Hesse, D. Winske, and J. Birn, Phys. Scr. **T74**, 63–66 (1998).
[48] J. D. B. Hodgson and T. Neukirch, Geophys. Astrophys. Fluid Dyn. **109**, 524–537 (2015).
[49] P. D. Hudson, Planet. Space Sci. **18**, 1611–1622 (1970).
[50] E. A. Kuznetsov, T. Passot, V. P. Ruban, and P. L. Sulem, Phys. Plasmas **22**(4), 042114 (2015).
[51] A. Le, W. Daughton, H. Karimabadi, and J. Egedal, Phys. Plasmas **23**(3), 032114 (2016).
[52] A. Le, J. Egedal, J. Ng, H. Karimabadi, J. Scudder, V. Roytershteyn, W. Daughton, and Y.-H. Liu, Phys. Plasmas **21**(1), 012103 (2014).
[53] A. Le, A. Stanier, W. Daughton, J. Ng, J. Egedal, W. D. Nystrom, and R. Bird, Phys. Plasmas **26**(10), 102114 (2019).
[54] B. Lembege and R. Pellat, Phys. Fluids **25**, 1995–2004 (1982).
[55] J. Liang, W. W. Liu, and E. F. Donovan, J. Geophys. Res. **114**, 10215, https://doi.org/10.1029/2009JA014357 (2009).
[56] S. Lu, A. V. Artemyev, V. Angelopoulos, Y. Lin, X. J. Zhang, J. Liu, L. A. Avanov, B. L. Giles, C. T. Russell, and R. J. Strangeway, J. Geophys. Res. **124**(2), 1052–1062, https://doi.org/10.1029/2018JA026202 (2019).
[57] S. Lu, Y. Lin, V. Angelopoulos, A. V. Artemyev, P. L. Pritchett, Q. Lu, and X. Y. Wang, J. Geophys. Res. **121**, 11, https://doi.org/10.1002/2016JA023325 (2016).
[58] A. T. Y. Lui, "Review on the characteristics of the current sheet in the earth's magnetotail," in *Electric Currents in Geospace and Beyond*, American Geophysical Union Geophysical Monograph Series Vol. 235, edited by A. Keiling, O. Marghitu, and M. Wheatland (AGU, Washington DC, 2018), pp. 155–175.
[59] M. V. Medvedev, V. I. Shevchenko, P. H. Diamond, and V. L. Galinsky, Phys. Plasmas **4**, 1257–1285 (1997).
[60] R. Nakamura, W. Baumjohann, Y. Asano, A. Runov, A. Balogh, C. J. Owen, A. N. Fazakerley, M. Fujimoto, B. Klecker, and H. RèMe, J. Geophys. Res. **111**, 11206, https://doi.org/10.1029/2006JA011706 (2006).
[61] R. Nakamura, W. Baumjohann, A. Runov, and Y. Asano, Space Sci. Rev. **122**, 29–38 (2006).
[62] A. I. Neishtadt, Regular Chaotic Dyn. **5**, 213–218 (2000).
[63] T. Neukirch, I. Y. Vasko, A. V. Artemyev, and O. Allanson, Astrophys. J **891**(1), 86 (2020).
[64] A. Noetzel, K. Schindler, and J. Birn, J. Geophys. Res. **90**, 8293–8300, https://doi.org/10.1029/JA090iA09p08293 (1985).
[65] E. N. Parker, *Spontaneous Current Sheets in Magnetic Fields: With Applications to Stellar X-rays*, International Series in Astronomy and Astrophysics Vol. 1 (Oxford University Press, New York, 1994).
[66] A. A. Petrukovich, A. V. Artemyev, I. Y. Vasko, R. Nakamura, and L. M. Zelenyi, Space Sci. Rev. **188**, 311–337 (2015).
[67] T. D. Phan, J. P. Eastwood, M. A. Shay, J. F. Drake, B. U. Ö. Sonnerup, M. Fujimoto, P. A. Cassak, M. Øieroset, J. L. Burch, R. B. Torbert, A. C. Rager, J. C. Dorelli, D. J. Gershman, C. Pollock, P. S. Pyakurel, C. C. Haggerty, Y. Khotyaintsev, B. Lavraud, Y. Saito, M. Oka, R. E. Ergun, A. Retino, O. Le Contel, M. R. Argall, B. L. Giles, T. E. Moore, F. D. Wilder, R. J. Strangeway, C. T. Russell, P. A. Lindqvist, and W. Magnes, Nature **557**(7704), 202–206 (2018).
[68] C. Pollock, T. Moore, A. Jacques, J. Burch, U. Gliese, Y. Saito, T. Omoto, L. Avanov, A. Barrie, V. Coffey, J. Dorelli, D. Gershman, B. Giles, T. Rosnack, C. Salo, S. Yokota, M. Adrian, C. Aoustin, C. Auletti, S. Aung, V. Bigio, N. Cao, M. Chandler, D. Chornay, K. Christian, G. Clark, G. Collinson, T. Corris, A. De Los Santos, R. Devlin, T. Diaz, T. Dickerson, C. Dickson, A. Diekmann, F. Diggs, C. Duncan, A. Figueroa-Vinas, C. Firman, M. Freeman, N. Galassi, K. Garcia, G. Goodhart, D. Guererro, J. Hageman, J. Hanley, E. Hemminger, M. Holland, M. Hutchins, T. James, W. Jones, S. Kreisler, J. Kujawski, V. Lavu, J. Lobell, E. LeCompte, A. Lukemire, E. MacDonald, A. Mariano, T. Mukai, K. Narayanan, Q. Nguyan, M. Onizuka, W. Paterson, S. Persyn, B. Piepgrass, F. Cheney, A. Rager, T. Raghuram, A. Ramil, L. Reichenthal, H. Rodriguez, J. Rouzaud, A. Rucker, Y. Saito, M. Samara, J.-A. Sauvaud, D. Schuster, M. Shappirio, K. Shelton, D. Sher, D. Smith, K. Smith, S. Smith, D. Steinfeld, R. Szymkiewicz, K. Tanimoto, J. Taylor, C. Tucker, K. Tull, A. Uhl, J. Vloet, P. Walpole, S. Weidner, D. White, G. Winkert, P.-S. Yeh, and M. Zeuch, Space Sci. Rev. **199**, 331–406 (2016).
[69] Z. J. Rong, S. Barabash, G. Stenberg, Y. Futaana, T. L. Zhang, W. X. Wan, Y. Wei, X. D. Wang, L. H. Chai, and J. Zhong, J. Geophys. Res. **120**, 5593–5602, https://doi.org/10.1002/2015JA021317 (2015).
[70] A. Runov, V. A. Sergeev, W. Baumjohann, R. Nakamura, S. Apatenkov, Y. Asano, M. Volwerk, Z. Vörös, T. L. Zhang, A. Petrukovich, A. Balogh, J. Sauvaud, B. Klecker, and H. Rème, Ann. Geophys. **23**, 1391–1403 (2005).
[71] A. Runov, V. A. Sergeev, R. Nakamura, W. Baumjohann, S. Apatenkov, Y. Asano, T. Takada, M. Volwerk, Z. Vörös, T. L. Zhang, J. Sauvaud, H. Rème, and A. Balogh, Ann. Geophys. **24**, 247–262 (2006).
[72] C. T. Russell, B. J. Anderson, W. Baumjohann, K. R. Bromund, D. Dearborn, D. Fischer, G. Le, H. K. Leinweber, D. Leneman, W. Magnes, J. D. Means, M. B. Moldwin, R. Nakamura, D. Pierce, F. Plaschke, K. M. Rowe, J. A. Slavin, R. J. Strangeway, R. Torbert, C. Hagen, I. Jernej, A. Valavanoglou, and I. Richter, Space Sci. Rev. **199**, 189–256 (2016).
[73] K. Schindler, "A self-consistent theory of the tail of the magnetosphere," in *Earth's Magnetospheric Processes*, Astrophysics and Space Science Library Vol. 32, edited by B. M. McCormac (Springer, Berlin, 1972), p. 200.
[74] K. Schindler, *Physics of Space Plasma Activity* (Cambridge University Press, 2006).
[75] K. Schindler and J. Birn, Phys. Rep. **47**, 109–165 (1978).
[76] K. Schindler and J. Birn, J. Geophys. Res. **107**, SMP 20-1, https://doi.org/10.1029/2001JA000304 (2002).
[77] K. Schindler, J. Birn, and M. Hesse, Phys. Plasmas **19**(8), 082904 (2012).
[78] I. P. Shkarofsky, T. W. Johnston, and M. P. Bachnynski, *The Particle Kinetic of Plasmas* (Addison-Wesley Piblishing Company, 1966).
[79] M. I. Sitnov and V. G. Merkin, J. Geophys. Res. **121**, 7664–7683, https://doi.org/10.1002/2016JA023001 (2016).
[80] M. I. Sitnov and K. Schindler, Geophys. Res. Lett. **37**, L08102, https://doi.org/10.1029/2010GL042961 (2010).
[81] M. I. Sitnov, M. Swisdak, P. N. Guzdar, and A. Runov, J. Geophys. Res. **111**, A08204, https://doi.org/10.1029/2005JA011517 (2006).
[82] S. I. Syrovatskii, Annu. Rev. Astron. Astrophys. **19**, 163–229 (1981).
[83] A. Tenerani and M. Velli, Astrophys. J. Lett. **867**(2), L26 (2018).
[84] A. Tenerani, M. Velli, and P. Hellinger, Astrophys. J. **851**, 99 (2017).
[85] R. B. Torbert, J. L. Burch, T. D. Phan, M. Hesse, M. R. Argall, J. Shuster, R. E. Ergun, L. Alm, R. Nakamura, K. J. Genestreti, D. J. Gershman, W. R. Paterson, D. L. Turner, I. Cohen, B. L. Giles, C. J. Pollock, S. Wang, L. J. Chen, J. E. Stawarz, J. P. Eastwood, K. J. Hwang, C. Farrugia, I. Dors, H. Vaith, C. Mouikis, A. Ardakani, B. H. Mauk, S. A. Fuselier, C. T. Russell, R. J. Strangeway, T. E. Moore, J. F. Drake, M. A. Shay, Y. V. Khotyaintsev, P. A. Lindqvist, W. Baumjohann, F. D. Wilder, N. Ahmadi, J. C. Dorelli, L. A. Avanov, M. Oka, D. N. Baker, J. F. Fennell, J. B. Blake, A. N. Jaynes, O. Le Contel, S. M. Petrinec, B. Lavraud, and Y. Saito, Science **362**(6421), 1391–1395 (2018).

[86] I. Y. Vasko, O. V. Agapitov, F. S. Mozer, J. W. Bonnell, A. V. Artemyev, V. V. Krasnoselskikh, G. Reeves, and G. Hospodarsky, Geophys. Res. Lett. **44**, 4575–4583, https://doi.org/10.1002/2017GL074026 (2017).

[87] A. P. Walsh, A. N. Fazakerley, C. Forsyth, C. J. Owen, M. G. G. T. Taylor, and I. J. Rae, J. Geophys. Res. **118**, 6042–6054, https://doi.org/10.1002/jgra.50553 (2013).

[88] A. P. Walsh, C. J. Owen, A. N. Fazakerley, C. Forsyth, and I. Dandouras, Geophys. Res. Lett. **38**, L06103, https://doi.org/10.1029/2011GL046770 (2011).

[89] C. Wang, M. Gkioulidou, L. R. Lyons, and V. Angelopoulos, J. Geophys. Res. **117**, A08215, https://doi.org/10.1029/2012JA017658 (2012).

[90] R. Wang, Q. Lu, R. Nakamura, W. Baumjohann, C. Huang, C. T. Russell, J. L. Burch, C. J. Pollock, D. Gershman, R. E. Ergun, S. Wang, P. A. Lindqvist, and B. Giles, Geophys. Res. Lett. **45**, 4542–4549, https://doi.org/10.1002/2017GL076330 (2018).

[91] R. Wang, I. Y. Vasko, and A. V. Artemyev, Phys. Plasmas **27**, 062901 (2020).

[92] E. Whipple, R. Puetter, and M. Rosenberg, Adv. Space Res. **11**, 133–142 (1991).

[93] P. H. Yoon and A. T. Y. Lui, J. Geophys. Res. **109**, A02210, https://doi.org/10.1029/2003JA010180 (2004).

[94] L. M. Zelenyi, A. V. Artemyev, H. V. Malova, and V. Y. Popov, J. Atmos. Sol.-Terr. Phys. **70**, 325–333 (2008).

[95] L. M. Zelenyi, A. G. Frank, A. V. Artemyev, A. A. Petrukovich, and R. Nakamura, Plasma Phys. Controlled Fusion **58**(5), 054002 (2016).

[96] L. M. Zelenyi, H. V. Malova, A. V. Artemyev, V. Y. Popov, and A. A. Petrukovich, Plasma Phys. Rep. **37**, 118–160 (2011).

[97] L. M. Zelenyi, H. V. Malova, V. Y. Popov, D. Delcourt, and A. S. Sharma, Nonlinear Processes Geophys. **11**, 579–587 (2004).

[98] L. M. Zelenyi, A. I. Neishtadt, A. V. Artemyev, D. L. Vainchtein, and H. V. Malova, Phys. Usp. **56**, 347–394 (2013).

[99] X. Zhou, V. Angelopoulos, A. Runov, M. I. Sitnov, F. Coroniti, P. Pritchett, Z. Y. Pu, Q.-G. Zong, J. P. McFadden, D. Larson, and K.-H. Glassmeier, J. Geophys. Res. **114**, A03223, https://doi.org/10.1029/2008JA013777 (2009).

[100] W. Zwingmann, J. Geophys. Res. **88**, 9101–9108, https://doi.org/10.1029/JA088iA11p09101 (1983).